Design and synthesis of new inhibitors of p53–MDM2 interaction with a chalcone scaffold

Pereira, Daniela; Lima, Raquel T.; Palmeira, Andreia; Seca, Hugo; Soares, Joana; Gomes, Sara

Published in:
Arabian Journal of Chemistry

DOI:
10.1016/j.arabjc.2016.04.015

Publication date:
2019

Arabian Journal of Chemistry (2019) 12, 4150–4161

King Saud University

Arabian Journal of Chemistry

www.ksu.edu.sa
www.sciencedirect.com

ORIGINAL ARTICLE

Design and synthesis of new inhibitors of p53–MDM2 interaction with a chalcone scaffold

Daniela Pereira [a,1], Raquel T. Lima [b,c,d,1], Andreia Palmeira [a], Hugo Seca [b,c], Joana Soares [e], Sara Gomes [e], Liliana Raimundo [e], Claudia Maciel [e], Madalena Pinto [a,f], Emília Sousa [a,f], M. Helena Vasconcelos [b,c,e], Lucília Saraiva [e,g,*], Honorina Cidade [a,f,*]

[a] *Laboratório de Química Orgânica e Farmacêutica, Departamento de Ciências Químicas, Faculdade de Farmácia, Universidade do Porto, Rua Jorge Viterbo Ferreira 228, 4050-313 Porto, Portugal*
[b] *i3S-Instituto de Investigação e Inovação em Saúde, Universidade do Porto, Portugal*
[c] *Cancer Drug Resistance Group, Institute of Molecular Pathology and Immunology of the University of Porto, IPATIMUP, Rua Júlio Amaral de Carvalho 45, 4200-135 Porto, Portugal*
[d] *Department of Pathology and Oncology, Faculty of Medicine of the University of Porto, Alameda Prof. Hernâni Monteiro, 4200-319 Porto, Portugal*
[e] *Laboratório de Microbiologia, Departamento de Ciências Biológicas, Faculdade de Farmácia, Universidade do Porto, Rua Jorge Viterbo Ferreira 228, 4050-313 Porto, Portugal*
[f] *Centro Interdisciplinar de Investigação Marinha e Ambiental (CIIMAR/CIMAR), Universidade do Porto, Rua dos Bragas 289, 4050-123 Porto, Portugal*
[g] *UCIBIO/REQUIMTE, Faculdade de Farmácia, Universidade do Porto, Rua de Jorge Viterbo Ferreira No. 228, 4050-313 Porto, Portugal*

Received 28 December 2015; accepted 23 April 2016
Available online 3 May 2016

KEYWORDS

Chalcones;
p53–MDM2 interaction inhibitors;

Abstract The virtual screening of a library of chalcone derivatives led us to the identification of potential new MDM2 ligands. The chalcones with the best docking scores obeying the Lipinski rule of five were subsequently prepared by base-catalyzed aldol reactions. The activity of these compounds as inhibitors of p53–MDM2 interaction was investigated using a yeast-based screening

* Corresponding authors at: Faculdade de Farmácia da Universidade do Porto, Laboratório de Microbiologia, Departamento de Ciências Biológicas, Rua Jorge Viterbo Ferreira n° 228 (E2), 4050-313 Porto, Portugal. Tel.: +351 220428584; fax: +351 226093390 (L. Saraiva). Faculdade de Farmácia da Universidade do Porto, Laboratório de Química Orgânica e Farmacêutica, Departamento de Ciências Químicas, Rua Jorge Viterbo Ferreira n° 228 (E2), 4050-313 Porto, Portugal. Tel.: +351 220428688; fax: +351 226093390 (H. Cidade).
E-mail addresses: lucilia.saraiva@ff.up.pt (L. Saraiva), hcidade@ff.up.pt (H. Cidade).
[1] Authors contributed equally to this work.

Peer review under responsibility of King Saud University.

Production and hosting by Elsevier

http://dx.doi.org/10.1016/j.arabjc.2016.04.015

In vitro antitumor activity; Docking

assay. Using this approach two chalcones (**3** and **4**) were identified as putative small molecule inhibitors of p53–MDM2 interaction. The activity of both chalcones was further investigated in a panel of human tumor cells. Chalcones **3** and **4** revealed a pronounced tumor cell growth inhibitory effect on tumor cell lines. Additionally, chalcone **4** caused alterations in the cell cycle profile, induced apoptosis and increased the levels of p53, p21 and PUMA proteins in NCI-H460 cells. Computational docking studies allowed to predict that, like nutlin-3A (a well-known small-molecule inhibitor of p53–MDM2 interaction), chalcones **3** and **4** bind to the p53-binding site of MDM2. The results here presented will be valuable for the structure-based design of novel and potent p53–MDM2 inhibitors.

1. Introduction

Despite the diversity of genes involved in tumorigenesis, the tumor suppressor protein p53 stands out as a master regulator of various signaling pathways involved in this process. p53 activation can prevent the proliferation of tumor cells by induction of cell growth arrest, senescence or apoptosis, modulation of the tumor stroma, as well as by inhibition of invasion and metastasis (Vousden and Prives, 2009). The p53 tumor suppressor pathway is one of the most frequently altered in human cancers. About half of all cancers retain wild-type p53, nevertheless the p53 pathway is inactivated due to the overexpression of the main endogenous negative regulator, murine double minute 2 (MDM2). MDM2 binds p53 and negatively regulates its activity, by direct inhibition of p53 transcriptional activity and enhancement of p53 degradation via the ubiquitin–proteasome pathway. The re-establishment of p53 activity by inhibition of its interaction with MDM2 represents an appealing therapeutic strategy for many wt p53 tumors with overexpression of MDM2, and has therefore been a focus of large effort in drug discovery (Kamal et al., 2012; Paiva et al., 2013; Selivanova, 2014; Wang et al., 2012).

Flavonoids have long been recognized for their broad spectrum of pharmacological activities (Erlund, 2004; Ferreira et al., 2014; Smejkal, 2014). Among this family of compounds, chalcones represent one of the major classes of naturally occurring products possessing a wide range of biological activities, namely antioxidant, antimicrobial, antiprotozoal, antimalarial, antiulcer, antihistaminic, anti-inflammatory, and antitumor activities (Mahapatra et al., 2015; Sahu et al., 2012; Singh et al., 2014). Some reports have related the antitumor activities of chalcones with activation of a p53-dependent pathway (Lai et al., 2014; Rao et al., 2010; Zhou and Ho, 2014). Additionally, it has been demonstrated that some chalcone derivatives can disrupt the p53–MDM2 complex with the subsequent release of p53 (Stoll et al., 2001). Together, these studies support the idea that chalcone may represent a promising chemical scaffold to search for new inhibitors of p53–MDM2 interaction.

Herein, potential novel MDM2 ligands were identified by virtual screening of a library of chalcones, and analysis of their activities as p53–MDM2 inhibitors was confirmed using a yeast-based cell assay. After analyzing their tumor cell growth inhibitory potential in a panel of human tumor cell lines, the activity of the most potent chalcones was further studied in the non-small cell lung cancer cell line (NCI-H460). The effect on cell proliferation, cell cycle, and apoptosis, as well as cellular levels of p53 and some of its downstream targets, was assessed for the most promising chalcone derivatives.

2. Material and methods

2.1. Docking of chalcones onto MDM2

The structures of 136 chalcones were drawn using Chemsketch (Advanced Chemistry Development, Inc. (ACD/Labs), Canada); the structure of the known p53–MDM2 inhibitor nutlin-3A was obtained from Pubchem (Wang et al., 2009). The 3-Dimensional (3D) structures of the chalcones and control were minimized by the semi-empirical Polak–Ribiere conjugate gradient method (RMS < 0.1 kcal $Å^{-1}$ mol^{-1}) using HyperChem 7.5 (Froimowitz, 1993).

The 3D structure of MDM2 was obtained from PDB (PDB id: 4HG7). Docking simulations between MDM2 and the small molecules were undertaken in AutoDock Vina (Scripps Research Institute, USA) (Seeliger and de Groot, 2010; Trott and Olson, 2009). AutoDock Vina considered the target conformation as a rigid unit while the ligands were allowed to be flexible and adaptable to the target. Vina searched for the lowest binding affinity conformations and returned nine different conformations for each ligand. AutoDock Vina was run using an exhaustiveness of 8 and a grid box with the dimensions 25.0, 20.0, 20.0, engulfing the cavity occupied by the crystallographic nutlin-3A (PDB id: 4HG7) (Anil et al., 2013). Conformations and interactions were visualized using PyMOL version 1.3 (Lill and Danielson, 2010). In order to validate the docking approach for the protein structure used, the respective co-crystallized known inhibitor, nutlin-3A (PDB id: 4HG7), was docked to the active site using Autodock Vina (supplementary data Fig. 1A); and a relation between docking scores and p53–MDM2 inhibitory activity was established (supplementary data Fig. 1B).

2.2. Synthesis

MW reactions were performed using a glassware setup for atmospheric pressure reactions and a 100 mL Teflon reactor (internal reaction temperature measurements with a fiber-optic probe sensor) and were carried out using an Ethos MicroSYNTH 1600 Microwave Labstation from Milestone. The reactions were monitored by thin-layer chromatography (TLC). Purifications of compounds were carried out by flash chromatography using Macherey–Nagel silica gel 60 (0.04–0.063 mm), and preparative thin-layer chromatography (TLC) using Macherey–Nagel silica gel 60 (GF_{254}) plates. Melting points were obtained in a Köfler microscope and are uncorrected. ^{1}H and ^{13}C NMR spectra were taken in $CDCl_3$ at room temperature, on Bruker Avance 300 and 500 instruments (300.13 MHz or 500.13 MHz for ^{1}H and 75.47 MHz or 125.77 MHz for ^{13}C). Chemical shifts are expressed in δ (ppm) values relative to tetramethylsilane (TMS) as an internal reference; ^{13}C NMR assignments were made by 2D (HSQC and HMBC) NMR experiments (long-range C, H coupling

constants were optimized to 7 Hz). HRMS mass spectra were recorded as ESI (electrospray ionization) mode on MicrOTOF spectrometer at C.A.C.T.I.-University of Vigo, Spain. 1-(2,4-Dihydroxy-3-propylphenyl)ethan-1-one, 3,4,5-trimethoxy, 3,4-dimethoxy-, 3,5-dimethoxy, 2,4-dimethoxy, 2,3-dimethoxy, and 2,4,5-trimethoxybenzaldehydes were purchased from Sigma Aldrich (Spain). The following materials were synthesized and purified by the described procedures.

2.2.1. Synthesis of 1-(2-hydroxy-4-methoxy-3-propylphenyl) ethan-1-one (*1*)

To a solution of 1-(2,4-dihydroxy-3-propylphenyl)ethan-1-one (**2**) (3.000 mmol, 0.584 g) in anhydrous acetone (20 mL) was added potassium carbonate (6 mmol, 0.8292 g). Dimethyl sulfate (342.7 μL) was added dropwise and the mixture was allowed to stir (4 h) at reflux and under nitrogen atmosphere. The reaction was quenched by the addition of about 80 mL of distilled water and acetone was evaporated. To the aqueous phase 1 M HCl was added to pH 2–3 and the solution extracted with ethyl acetate (3 × 100 mL). The organic phase was washed with brine (2 × 50 mL) and dried over anhydrous sodium sulfate. The organic solvent was evaporated and 1-(2-hydroxy-4-methoxy-3-propylphenyl)ethan-1-one (**1**) was obtained in quantitative yield.

2.2.1.1. 1-(2-hydroxy-4-methoxy-3-propylphenyl)ethan-1-one (1). ^{1}H NMR ($CDCl_3$, 300.13 MHz): δ 12.73 (1H, s, 2-OH), 7.60 (1H, d, J = 8.9 Hz, H-6), 6.45 (1H, d, J = 8.9 Hz, H-5), 3.88 (3H, s, 4-OCH_3), 2.62 (2H, t, J = 6.0 Hz, H-1″), 2.57 (3H, s, $COCH_3$), 1.46–1.59 (2H, m, H-2″), 0.97 (3H, t, J = 7.4 Hz, H-3″). ^{13}C NMR ($CDCl_3$, 75.47 MHz): δ 202.9 (CO), 163.5 (C-2), 162.0 (C-4), 130.0 (C-6), 118.3 (C-1), 114.2 (C-3), 101.9 (C-5), 55.7 (OCH_3), 26.3 ($COCH_3$), 24.3 (C-1″), 21.9 (C-2″), 14.2 (C-3″).

2.2.2. General procedure for the synthesis of chalcones *3*–*8*

To a solution of 1-(2-hydroxy-4-methoxy-3-propylphenyl)eth an-1-one (**1**) (1.000 mmol, 0.208 g) in methanol was added an aqueous solution of sodium hydroxide (60%) to pH 13–14. Then, a solution of 2 mmol of the appropriate benzaldehyde in methanol was slowly added to the reaction mixture. The reaction was submitted to successive 15 min periods of microwave irradiation of 180 W of power. Total irradiation time was 60 (chalcone **8**) or 90 min (chalcones **3**–**7**) and the final temperature was 75 °C. The solution was extracted with chloroform (3 × 50 mL). The combined organic layers were rinsed with brine and water, dried over anhydrous sodium sulfate and evaporated under reduced pressure. The obtained residues were purified as indicated below for the referred chalcones.

2.2.2.1. (E)-1-(2-hydroxy-4-methoxy-3-propylphenyl)-3-(3,4, 5-trimethoxyphenyl)prop-2-en-1-one (3). Purified by flash column chromatography (*n*-hexane:ethyl acetate, 9:1) followed by crystallization (chloroform). Yield: 37% as yellow crystals; mp (chloroform): 126.0–127.2 °C; ^{1}H NMR ($CDCl_3$, 300.13 MHz): δ 13.38 (1H, s, 2′-OH), 7.81 (1H, d, J = 9.2 Hz, H-6′), 7.80 (1H, d, J = 15.0 Hz, H-β), 7.49 (1H, d, J = 15.0 Hz, H-α), 6.87 (2H, s, H-2,6), 6.51 (1H, d, J = 9.2 Hz, H-5′), 3.94 (6H, s, 3-,5-OCH_3), 3.91 (6H, s, 4-,4′-OCH_3), 2.66 (2H, t, J = 7.7 Hz, H-1″), 1.59–1.52 (2H, m, H-2″), 0.97 (3H, t, J = 7.4 Hz, H-3″); ^{13}C NMR ($CDCl_3$, 75.47 MHz): δ 192.1 (CO), 163.6 (C-4′), 163.3 (C-2′), 153.5 (C-3,5), 144.2 (C-β), 140.4 (C-4), 130.4 (C-1), 129.0 (C-6′), 119.8 (C-α), 118.6 (C-3′), 114.4 (C-1′), 105.7 (C-2,6), 102.0 (C-5′), 61.0 (4-OCH_3), 56.2 (3,5-OCH_3), 55.7 (4′-OCH_3), 24.4 (C-1″), 21.9 (C-2″), 14.2 (C-3″); ESI-HRMS (+) m/z: Anal. Calc. for $C_{22}H_{27}O_6$ $(M+H)^+$: 387.18022; found: 387.18050.

2.2.2.2. (E)-3-(3,4-dimethoxyphenyl)-1-(2-hydroxy-4-methoxy-3-propylphenyl)prop-2-en-1-one (4). Purified by flash column chromatography (*n*-hexane:ethyl acetate, 9:1). Yield: 42% as yellow solid; mp (n-hexane: ethyl acetate): 122.6–125.7 °C; ^{1}H NMR ($CDCl_3$, 500.13 MHz): δ 13.46 (1H, s, 2′-OH), 7.84 (1H, d, J = 15.4 Hz, H-β), 7.81 (1H, d, J = 9.1 Hz, H-6′), 7.48 (1H, d, J = 15.4 Hz, H-α), 7.25 (1H, dd, J = 8.5, 1.9 Hz, H-6), 7.16 (1H, d, J = 1.9 Hz, H-2), 6.91 (1H, d, J = 8.5 Hz, H-5), 6.50 (1H, d, J = 9.1 Hz, H-5′), 3.97 (3H, s, 3-OCH_3), 3.94 (3H, s, 4-OCH_3), 3.90 (3H, s, 4′-OCH_3), 2.65 (2H, t, J = 7.6 Hz, H-1″), 1.58–1.52 (2H, m, H-2″), 0.97 (3H, t, J = 7.3 Hz, H-3″); ^{13}C NMR ($CDCl_3$, 125.77 MHz): δ 192.2 (CO), 163.4 (C-4′), 163.2 (C-2′), 151.4 (C-4), 149.2 (C-3), 144.2 (C-β), 128.9 (C-6′), 127.8 (C-1), 123.2 (C-6), 118.5 (C-3′), 118.3 (C-α), 114.5 (C-1′), 111.0 (C-5), 110.1 (C-2), 101.9 (C-5′), 56.0 (4-OCH_3), 55.9 (3-OCH_3), 55.7 (4′-OCH_3), 24.4 (C-1″), 21.9 (C-2″), 14.3 (C-3″); ESI-HRMS (+) m/z: Anal. Calc. for $C_{21}H_{25}O_5$ $(M+H)^+$: 357.16965; found: 357.16957.

2.2.2.3. (E)-3-(2,3-dimethoxyphenyl)-1-(2-hydroxy-4-methoxy-3-propylphenyl)prop-2-en-1-one (5). Purified by flash column chromatography (petroleum ether:diethyl ether, 5:5). Yield: 35% as yellow solid; mp (petroleum ether: diethyl ether): 103.0–104.5 °C; ^{1}H NMR ($CDCl_3$, 500.13 MHz): δ 13.39 (1H, s, 2′-OH), 8.14 (1H, d, J = 15.6 Hz, H-β), 7.79 (1H, d, J = 9.0 Hz, H-6′), 7.71 (1H, d, J = 15.6 Hz, H-α), 7.27 (1H, d, J = 8.0 Hz, H-6), 7.11 (1H, t, J = 8.0 Hz, H-5), 6.97 (1H, d, J = 8.0 Hz, H-4), 6.49 (1H, d, J = 9.0 Hz, H-5′), 3.90 (9H, s, 2-,3-,4′-OCH_3), 2.65 (2H, t, J = 7.6 Hz, H-1″), 1.52–1.58 (2H, m, H-2″), 0.96 (3H, t, J = 7.4 Hz, H-3″); ^{13}C NMR ($CDCl_3$, 75.47 MHz): δ 192.6 (CO), 163.5 (C-4′), 163.3 (C-2′), 153.2 (C-3), 148.9 (C-2), 138.9 (C-β), 129.2 (C-1), 129.1 (C-6′), 124.2 (C-5), 122.3 (C-α), 119.8 (C-6), 118.5 (C-3′), 114.5 (C-1′), 114.1 (C-4), 102.0 (C-5′), 61.3 (2-OCH_3), 55.9 (3-OCH_3), 55.7 (4′-OCH_3), 24.4 (C-1″), 21.9 (C-2″), 14.2 (C-3″); ESI-HRMS (+) m/z: Anal. Calc. for $C_{21}H_{25}O_5$ $(M+H)^+$: 357.16965; found: 357.16964.

2.2.2.4. (E)-1-(2-hydroxy-4-methoxy-3-propylphenyl)-3-(2,4, 5-trimethoxyphenyl)prop-2-en-1-one (6). Purified by flash column chromatography (petroleum ether:chloroform, 5:5) followed by thin layer chromatography (petroleum ether: chloroform, 2:8). Yield: 34% as dark yellow solid; mp (petroleum ether: diethyl ether): 106.0–107.0 °C; ^{1}H NMR ($CDCl_3$, 500.13 MHz): δ 13.60 (1H, s, 2′-OH), 8.16 (1H, d, J = 15.5 Hz, H-β), 7.80 (1H, d, J = 9.0 Hz, H-6′), 7.57 (1H, d, J = 15.5 Hz, H-α), 7.12 (1H, s, H-6), 6.53 (1H, s, H-3), 6.49 (1H, d, J = 9.0 Hz, H-5′), 3.95 (3H, s, 4-OCH_3), 3.92 (3H, s, 5-OCH_3), 3.91 (3H, s, 2-OCH_3), 3.89 (3H, s, 4′-OCH_3), 2.65 (2H, t, J = 7.6 Hz, H-1″), 1.59–1.49 (2H, m, H-2″), 0.97 (3H, t, J = 7.3 Hz, H-3″); ^{13}C NMR ($CDCl_3$, 75.47 MHz): δ 192.7 (CO), 163.2 (C-4′), 163.1 (C-2′), 154.7 (C-2), 152.5 (C-4), 143.1 (C-5), 139.5 (C-β), 128.9 (C-6′), 118.4 (C-α), 118.3 (C-3′), 114.6 (C-1′), 111.6 (C-6), 108.9

(C-1), 101.7 (C-5′), 96.6 (C-3), 56.5 (2-OCH_3), 56.3 (4-OCH_3), 56.0 (5-OCH_3), 55.6 (4′-OCH_3), 24.4 (C-1″), 21.9 (C-2″), 14.3 (C-3″); ESI-HRMS (+) *m/z*: Anal. Calc. for $C_{22}H_{27}O_6$ $(M+H)^+$: 387.18022; found: 387.18018.

2.2.2.5. (E)-3-(3,5-dimethoxyphenyl)-1-(2-hydroxy-4-methoxy-3-propylphenyl)prop-2-en-1-one (7). Purified by flash column chromatography (*n*-hexane:ethyl acetate, 9:1). Yield: 37% as yellow solid; mp (n-hexane:ethyl acetate): 122.6–125.7 °C; ^{1}H NMR ($CDCl_3$, 500.13 MHz): δ 13.33 (1H, s, 2′-OH), 7.79 (1H, d, *J* = 15.4 Hz, H-β), 7.78 (1H, d, *J* = 9.0 Hz, H-6′), 7.56 (1H, d, *J* = 15.4 Hz, H-α), 6.78 (2H, d, *J* = 2.2 Hz, H-2,6), 6.53 (1H, t, *J* = 2.2 Hz, H-4), 6.50 (1H, d, *J* = 9.0 Hz, H-5′), 3.90 (3H, s, 4′-OCH_3), 3.84 (3H, s, 3-OCH_3), 3.80 (3H, s, 5′-OCH_3), 2.66 (2H, t, *J* = 7.6 Hz, H-1″), 1.59–1.53 (2H, m, H-2″), 0.96 (3H, t, *J* = 7.3 Hz, H-3″); ^{13}C NMR ($CDCl_3$, 75.47 MHz): *δ* 192.2 (CO), 163.6 (C-4′), 163.3 (C-2′), 161.0 (C-3,5), 144.0 (C-β), 136.7 (C-1), 129.1 (C-6′), 121.1 (C-α), 118.5 (C-3′), 114.4 (C-1′), 106.4 (C-2,6), 102,5 (C-4), 102.0 (C-5′), 55.7 (3,4′-OCH_3), 55.5 (5-OCH_3), 24.4 (C-1″), 21.9 (C-2″), 14.2 (C-3″); ESI-HRMS (+) *m/z*: Anal. Calc. for $C_{21}H_{25}O_5$ $(M+H)^+$: 357.16965; found: 357.16909.

2.2.2.6. (E)-3-(2,4-dimethoxyphenyl)-1-(2-hydroxy-4-methoxy-3-propylphenyl)prop-2-en-1-one (8). Purified by flash column chromatography (*n*-hexane:ethyl acetate, 9:1). Yield: 33% as yellow solid; mp (n-hexane:ethyl acetate): 152.0–152.5 °C; ^{1}H NMR ($CDCl_3$, 300.13 MHz): *δ* 8.12 (1H, d, *J* = 15.5 Hz, H-β), 7.80 (1H, d, *J* = 8.9 Hz, H-6′), 7.64 (1H, d, *J* = 15.5 Hz, H-α), 7.58 (1H, d, *J* = 8.6 Hz, H-6), 6.55 (1H, dd, *J* = 8.6, 2.4 Hz, H-5), 6.49 (1H, d, *J* = 8.9 Hz, H-5′), 6.48 (1H, d, *J* = 2.4 Hz, H-3), 3.92 (3H, s, 4′-OCH_3), 3.89 (3H, s, 4-OCH_3), 3.86 (3H, s, 2-OCH_3), 2.66 (2H, t, *J* = 7.6 Hz, H-1″), 1.62–1.49 (2H, m, H-2″), 0.97 (3H, t, *J* = 7.4 Hz, H-3″); ^{13}C NMR ($CDCl_3$, 75 MHz): δ 192.9 (CO), 163.2 (C-4,4′), 163.0 (C-2′), 160.4 (C-2), 139.8 (C-β), 131.1 (C-6), 128.9 (C-6′), 118.6 (C-3′), 118.4 (C-α), 117.1 (C-1), 114.7 (C-1′), 105.4 (C-5), 101.7 (C-5′), 98.4 (C-3), 55.6 (4′-OCH_3), 55.5 (2,4-OCH_3), 24.4 (C-1″), 21.9 (C-2″), 14.3 (C-3″) (the *δ* value for O<u>H</u> is not visible probably due to exchange with hydrochloric acid in the solvent used, $CDCl_3$); ESI-HRMS (+) *m/z*: Anal. Calc. for $C_{21}H_{25}O_5$ $(M+H)^+$: 357.16965; found: 357.16942.

2.2.3. Synthesis of chalcones 9–12, 16 and 17

Chalcones **9** (58%), **10** (34%), **11** (28%), **12** (26%), **16** (35%), and **17** (53%) were synthesized and characterized according to the previously described procedure (Neves et al., 2012a).

2.2.3.1. (E)-3-(4-(benzyloxy)phenyl)-1-(2,4-dihydroxyphenyl) prop-2-en-1-one (9). ^{1}H NMR ($CDCl_3$, 300 MHz): *δ* 13.47 (1H, s, 2′-OH), 7.86 (1H, d, *J* = 15.3 Hz, H-β), 7.83 (1H, d, *J* = 9.4 Hz, H-6′), 7.62 (2H, d, *J* = 8.7 Hz, H-2,6), 7.46 (1H, d, *J* = 15.3 Hz, H-α), 7.46–7.33 (5H, m, 4-OBn), 7.02 (2H, d, *J* = 8.7 Hz, H-3,5), 6.44 (1H, dd, *J* = 9.4, 2.4 Hz, H-5′), 6.42 (1H, d, *J* = 2.4 Hz, H-3′), 5.88 (1H, br s, 4′-OH), 5.13 (2H, s, 4-OCH_2). ESI-HRMS (+) *m/z*: Anal. Calc for $C_{22}H_{19}O_4$ $(M+H)^+$: 347.1278; found: 347.1276.

2.2.3.2. (E)-1-(2,4-dihydroxy-3-propylphenyl)-3-(3,4,5-trimethoxyphenyl)prop-2-en-1-one (10). ^{1}H NMR ($CDCl_3$, 300 MHz): *δ* 13.68 (1H, s, 2′-OH), 7.80 (1H, d, *J* = 15.4 Hz, H-β), 7.72 (1H, d, *J* = 8.9 Hz, H-6′), 7.46 (1H, d, *J* = 15.4 Hz, H-α), 6.86 (2H, s, H-2,6), 6.43 (1H, d, *J* = 8.9 Hz, H-5′), 5.78 (1H, br s, 4′-OH), 3.93 (6H, s, 3,5-OCH_3), 3.91 (3H, s, 4-OCH_3), 2.67 (2H, t, *J* = 7.7 Hz, H-1″), 1.68–1.56 (2H, m, H-2″), 1.00 (3H, t, *J* = 7.4 Hz, H-3″); ESI-HRMS (+) *m/z*: Anal. Calc for $C_{21}H_{25}O_6$ $(M+H)^+$: 313.1646; found: 313.1643.

2.2.3.3. (E)-1-(2,4-dihydroxy-3-propylphenyl)-3-(2,4,5-trimethoxyphenyl)prop-2-en-1-one (11). ^{1}H NMR ($CDCl_3$, 300 MHz): *δ* 13.89 (1H, s, 2′-OH), 8.17 (1H, d, *J* = 15.5 Hz, H-β), 7.72 (1H, d, *J* = 8.9 Hz, H-6′), 7.55 (1H, d, *J* = 15.5 Hz, H-α), 7.12 (1H, s, H-6), 6.53 (1H, s, H-3), 6.41 (1H, d, *J* = 8.9 Hz, H-5′), 5.44 (1H, br s, 4′-OH), 3.96 (3H, s, 2-OCH_3), 3.93 (3H, s, 5-OCH_3), 3.92 (3H, s, 4-OCH_3), 2.66 (2H, t, *J* = 7.7 Hz, H-1″), 1.66–1.56 (2H, m, H-2″); 1.00 (3H, t, *J* = 7.4 Hz, H-3″). ESI-HRMS (+) *m/z*: Anal. Calc for $C_{21}H_{25}O_6$ $(M+H)^+$: 373.1646; found: 373.1643.

2.2.3.4. (E)-1-(2,4-dihydroxy-3-propylphenyl)-3-(4-methoxyphenyl)prop-2-en-1-one (12). ^{1}H NMR ($CDCl_3$, 300 MHz): *δ* 13.78 (1H, s, 2′-OH), 7.86 (1H, d, *J* = 15.4 Hz, H-β), 7.72 (1H, d, *J* = 8.9 Hz, H-6'), 7.61 (2H, d, *J* = 8.8 Hz, H-2,6), 7.24 (1H, d, *J* = 15.4 Hz, H-α), 6.95 (2H, d, *J* = 8.8 Hz, H-3,5), 6.41 (1H, d, *J* = 8.9 Hz, H-5′), 5.39 (1H, br s, 4′-OH), 3.87 (3H, s, 4-OCH_3), 2.66 (2H, t, *J* = 7.7 Hz, H-1″), 1.65–1.58 (2H, m, H-2″), 1.00 (3H, t, *J* = 7.4 Hz, H-3″). ESI-HRMS (+) *m/z*: Anal. Calc for $C_{19}H_{21}O_4$ $(M+H)^+$: 313.1434; found: 313.1435.

2.2.3.5. (E)-1-(2,4-dihydroxyphenyl)-3-(3,4,5-trimethoxyphenyl)prop-2-en-1-one (16). ^{1}H NMR ($CDCl_3$, 500 MHz): *δ* 13.38 (1H, s, 2′-OH), 7.85 (1H, d, *J* = 8.6 Hz, H-6′), 7.81 (1H, d, *J* = 15.3 Hz, H-β), 7.45 (1H, d, *J* = 15.3 Hz, H-α), 6.87 (2H, s, H-2,6), 6.45 (1H, dd, *J* = 8.6, 2.5 Hz, H-5′), 6.43 (1H, d, *J* = 2.5 Hz, H-3′), 3.94 (6H, s, 3,5-OCH_3), 3.91 (3H, s, 4-OCH_3). ESI-HRMS (+) *m/z*: Anal. Calc for $C_{18}H_{19}O_6$ $(M+H)^+$: 331.1176; found: 331.1177.

2.2.3.6. (E)-1-(2,4-dihydroxyphenyl)-3-(2,4,5-trimethoxyphenyl)prop-2-en-1-one (17). ^{1}H NMR ($CDCl_3$, 500 MHz): *δ* 8.18 (1H, d, *J* = 15.4 Hz, H-β), 7.84 (1H, d, *J* = 8.3 Hz, H-6′), 7.53 (1H, d, *J* = 15.4 Hz, H-α), 7.12 (1H, s, H-6), 6.53 (1H, s, H-3), 6.43 (1H, dd, *J* = 8.3, 2.5 Hz, H-5′), 6.42 (1H, d, *J* = 2.5 Hz, H-3′), 3.96 (3H, s, 2-OCH_3), 3.93 (3H, s, 5-OCH_3), 3.92 (3H, s, 4-OCH_3) (the *δ* value for O<u>H</u> is not visible probably due to exchange with hydrochloric acid in the solvent used, $CDCl_3$); ESI-HRMS (+) *m/z*: Anal. Calc for $C_{18}H_{19}O_6$ $(M+H)^+$: 331.1176; found: 331.1175.

2.3. Biological evaluation

2.3.1. Yeast strains and growth conditions

For the yeast growth-inhibition assay, co-transformed *Saccharomyces cerevisiae* cells expressing human MDM2 and/or human p53 and control yeasts (co-transformed with the empty vectors pLS239 and pGADT7) obtained in previous work (Leao et al., 2013) were used. For selection of co-transformed yeasts, cells were routinely grown in a minimal selective medium with 2% (w/w) glucose, 0.7% (w/w) yeast

nitrogen base without amino acids from Difco (Quilaban, Sintra, Portugal) and all the amino acids required for yeast growth (50 μg/mL) except leucine and tryptophan, to approximately 1 optical density at 600 nm (OD_{600}). To induce expression of wt p53 and MDM2, yeasts were diluted to 0.05 OD_{600} into selective induction medium with 2% (w/w) galactose and 2% (w/w) raffinose (instead of glucose), and incubated at 30 °C under continuous orbital shaking (200 r.p.m.) for approximately 42 h (time required by control yeast, to achieve 0.45 OD_{600}). Yeast growth was analyzed by counting the number of colony-forming units (CFU) per mL (CFU/mL) after 2 days incubation at 30 °C on Sabouraud Dextrose Agar plates from Liofilchem (Frilabo, Porto, Portugal).

2.3.2. Effects of compounds on yeast cell growth

Co-transformed yeast cells were incubated in selective induction medium in the presence of 10 μM nutlin-3A (Sigma), 1–50 μM of each compound or 0.1% DMSO only, for approximately 42 h, at 30 °C, under continuous orbital shaking. Yeast cell growth was analyzed as described in Section 3.3.1. Results were estimated considering as 100% growth the number of CFU obtained with the control yeast.

2.3.3. Studies in human tumor cell lines

2.3.3.1. Cell culture. The following human tumor cell lines were used: MCF-7 (breast cancer), NCI-H460 (non-small cell lung cancer), AGS (gastric cancer) and the HCT116 $p53^{+/+}$ and $p53^{-/-}$ isogenic cells (colon cancer). The cell lines were routinely maintained in RPMI-1640 medium with UltraGlutamine I and 25 mM Hepes (Lonza), supplemented with 10% heat-inactivated fetal bovine serum (FBS, Biowest) at 37 °C in a humidified atmosphere containing 5% CO_2. Cell number and viability were assessed using trypan blue (Sigma). All the experiments were performed with exponentially growing cells presenting more than 90% cell viability.

2.3.3.2. In vitro cell growth inhibition screening assay. Cells were plated in a 5% FBS supplemented medium in 96-well plates (5000 cells/well for MCF-7, NCI-H460 and HCT116 cells and 7500 cells/well for AGS cells) and then allowed to adhere for 24 h. Cells were then treated with five serial dilution concentrations of each compound (from a maximum concentration of 150 μM). Following a 48 h incubation period, cells were fixed in situ with 10% ice cold trichloroacetic acid, washed and stained with Sulforhodamine B (SRB) (Neves et al., 2011; Neves et al., 2012a, 2012b). The bound stain was solubilized in 10 mM Tris-base and the absorbance was measured at 510 nm in a multiwell plate reader (Biotek Instruments Inc. Synergy Mx, USA). The effect of maximum volume of DMSO (solvent, 0.25%) was analyzed in all experiments.

2.3.3.3. Effect of compounds 3 and 4 in NCI-H460 viable cell number, cell cycle profile, apoptosis and protein expression. *2.3.3.3.1. Cell treatments*. NCI-H460 cells were plated in 6-well plates (1×10^5 cells/well) in a 10% FBS supplemented medium, at 37 °C, in a humidified incubator with 5% CO_2, for 24 h. Cells were then treated for 48 h to the GI_{50} and $2xGI_{50}$ concentrations of compounds **3** and **4**, corresponding respectively to 2.1 μM and 4.2 μM of compound **3** and 3.3 μM and 6.6 μM of compound **4**. Cells were also incubated with medium only (Blank) or with the highest volume of DMSO used (0.11%). Following treatment, viable cell number and viability were determined with the Trypan blue exclusion assay and cells were further processed as follows.

2.3.3.3.2. Cell cycle profile. Following 48 treatment, cell pellets were fixed in ice-cold 70% ethanol and stored at 4 °C. For analysis, cells were incubated in 5 μg/mL propidium iodide and 100 μg/mL RNase A (in PBS) for 30 min on ice. Analysis of cellular DNA content was carried out using a BD Accuri C6 cytometer (BD Biosciences). The percentage of cells in the different phases of the cell cycle (G1, S and G2/M phases) was carried out after exclusion of cell debris and aggregates, using the FlowJo 7.6.5 software (Tree Star, Inc., Ashland, OR, USA) (Cazal et al., 2013). At least 20,000 events were analyzed for each of the conditions.

2.3.3.3.3. BrdU incorporation assay. Following 47 h treatment, cells were incubated with 10 μM bromodeoxyuridine (BrdU; Sigma) for 1 h. Cells were then trypsinized and fixed in 4% paraformaldehyde (in PBS) for 30 min. Cytopsins were prepared and cells were incubated for 20 min in 2 M HCl for denaturation. After incubation with mouse anti-BrdU primary antibody (1/10, Dako) for 1 h at room temperature and further incubation with anti-mouse-Ig-FITC (1/100, Dako) for 30 min, at room temperature, slides were mounted with Vectashield mounting medium with DAPI (Vector Laboratories). BrdU incorporation was determined by counting a minimum of 500 cells per slide using a fluorescence microscope (DM2000; LEICA) (Preto et al., 2009).

2.3.3.3.4. Apoptosis. Following 48 h treatment, cellular apoptosis levels were assessed using the "Human AnnexinV-FITC/PI apoptosis" kit (Bender MedSystems) as previously described (Neves et al., 2011). Briefly, cell pellets were resuspended in binding buffer (diluted in H_2O) and incubated with Annexin V-FITC and with propidium iodide. Samples were analyzed using a BD Accuri C6 cytometer (BD Biosciences). The FlowJo 7.6.5 software (Tree Star, Inc., Ashland, OR, USA) was used and at least 20,000 events were analyzed for each condition.

2.3.3.3.5. Protein expression. Total protein lysates were prepared by lysing cells in Winman's buffer (1% NP-40, 0.1 M Tris–HCl pH 8.0, 0.15 M NaCl and 5 mM EDTA) with protease inhibitor cocktail (Roche) (Lima et al., 2006). Protein content was quantified with DC™ Protein Assay kit (Biorad) according to manufacturer's instructions. Proteins were electrophoretically separated on 12% SDS–PAGE gel and transferred into nitrocellulose membranes (Amersham). Membranes were incubated with the following primary antibodies: mouse anti-p53 (DO-1, 1:5000, Santa Cruz Biotechnology), mouse anti-p21 (1:250, Calbiochem), mouse anti-PUMA (1:500, Santa Cruz Biotechnology) and goat anti-Actin antibody (1:2000, Santa Cruz Biotechnology) and with the corresponding secondary antibody: donkey anti-goat IgG-HRP (1:2000, Santa Cruz Biotechnology) or goat anti-mouse IgG-HRP (1:2000, Santa Cruz Biotechnology). Signal was detected using Amersham™ ECL Western Blotting Detection Reagents (GE Healthcare), the Amersham Hyperfilm ECL (GE Healthcare) and the Kodak GBX developer and fixer (Sigma). The intensity of the bands obtained in each film was further ana-

lyzed using the software Quantity One – 1D Analysis (Bio-Rad, USA).

2.4. Statistical analysis

All data are presented as mean ± SEM from at least three independent experiments. Statistical analysis was carried out using an unpaired student's *t*-test. * Indicates $p \leqslant 0.05$ and ** $p \leqslant 0.01$ between blank cells (cells treated with medium only) and each treatment.

3. Results and discussion

3.1. Virtual screening

p53–MDM2 interaction is mediated by a well-defined hydrophobic surface pocket in MDM2 and three key hydrophobic residues in p53, namely Phe-19, Trp-23, and Leu-26 (Kussie et al., 1996; Ma et al., 2005). Therefore, small-molecules with a chalcone scaffold may be designed in order to block this interaction to reactivate p53 in cells harboring wt p53 (Fotouhi and Graves, 2005; Secchiero et al., 2011).

As a part of an ongoing effort to identify new disruptors of the MDM2–p53 interaction for potential drug development (Leao et al., 2013), virtual screening was performed on 136 newly designed chalcones. This library of virtual chalcones was submitted to a docking study using MDM2 as target. Several chalcones presented docking scores similar to the known p53–MDM2 inhibitor nutlin-3A. The best scoring molecules (docking scores $\leqslant -7$ kcal/mol) are represented on Table 1. The docking scores of the 125 chalcones with docking scores > -7 kcal/mol are represented in Supplementary Table 1. The chalcones with docking scores lower or equal to -7 kcal/mol which respected Lipinski rule of five were subsequently synthetized. In order to understand the relationship between docking scores, docking poses, and% of p53–MDM2 inhibitory activity, structure-related chalcones with lower docking scores were also synthesized and tested.

Table 1 Best scoring small molecules (from a virtual library of chalcones) that resulted from a docking simulation using MDM2 as target.

Ligand	Docking score (kcal/mol)
(*E*)-1-(2-hydroxy-4-methoxy-3-propylphenyl)-3-(3,4,5-trimethoxyphenyl)prop-2-en-1-one (**3**)	−7.5
(*E*)-3-(3,4-dimethoxyphenyl)-1-(2-hydroxy-4-methoxy-3-propylphenyl)prop-2-en-1-one (**4**)	−7.5
(*E*)-3-(2,3-dimethoxyphenyl)-1-(2-hydroxy-4-methoxy-3-propylphenyl)prop-2-en-1-one (**5**)	−7
(*E*)-1-(2-hydroxy-4-methoxy-3-propylphenyl)-3-(2,4,5-trimethoxyphenyl)prop-2-en-1-one (**6**)	−7
(*E*)-3-(4-(benzyloxy)phenyl)-1-(2,4-dihydroxyphenyl)prop-2-en-1-one (**9**)	−8.3
(*E*)-1-(2,4-dihydroxy-3-propylphenyl)-3-(3,4,5-trimethoxyphenyl)prop-2-en-1-one (**10**)	−7.5
(*E*)-1-(2,4-dihydroxy-3-propylphenyl)-3-(2,4,5-trimethoxyphenyl)prop-2-en-1-one (**11**)	−7.1
(*E*)-1-(2,4-dihydroxy-3-propylphenyl)-3-(4-methoxyphenyl)prop-2-en-1-one (**12**)	−7
(*E*)-3-(4-(benzyloxy)phenyl)-1-(2,4-dihydroxy-3-methylphenyl)prop-2-en-1-one (**13**)[a]	−8.3
(*E*)-1-(2,4-dihydroxy-3-propylphenyl)-3-(4-(trifluoromethyl)phenyl)prop-2-en-1-one (**14**)[a]	−7.8
(*E*)-3-(2-chlorophenyl)-1-(2,4-dihydroxy-3-propylphenyl)prop-2-en-1-one (**15**)[a]	−7.7
Nutlin-3A (control)	−7.6

[a] Molecules with LogP greater than 5 (excluded for not obeying Lipinski rule of five). LogP was determined using the atom-based octanol–water partition coefficient implemented by Ghose and Crippen (Ghose and Crippen, 1987).

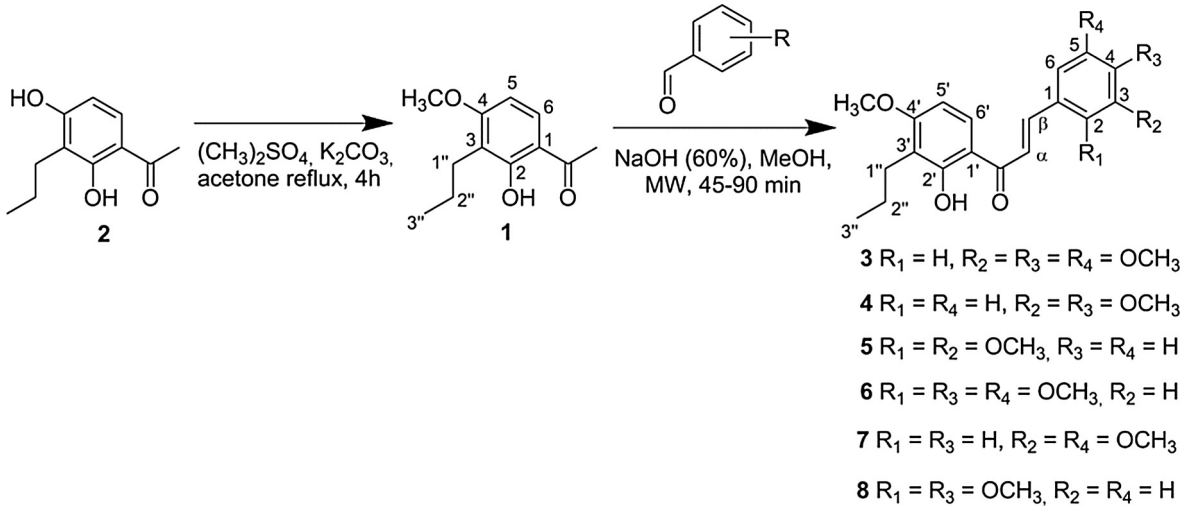

Scheme 1 Synthesis of chalcones **3**–**8**. The numbering used concerns the NMR assignments.

3.2. Chemistry

Six new chalcone derivatives **3**–**8** were prepared by base-catalyzed aldol reactions of 1-(2-hydroxy-4-methoxy-3-propyl phenyl)ethan-1-one (**1**) with appropriately substituted benzaldehydes as building blocks by MAOS, according to the strategy illustrated on Scheme 1. 1-(2-Hydroxy-4-methoxy-3-propylphenyl)ethan-1-one (**1**) was synthesized by the methylation of 1-(2,4-dihydroxy-3-propylphenyl)ethan-1-one (**2**) with dimethyl sulfate in presence of anhydrous potassium carbonate and anhydrous acetone (Scheme 1). The structure elucidation of compound **1** was established by ^{1}H and ^{13}C NMR techniques and data were in accordance to the previously reported (Alves de Lima et al., 1982; Alves de Lima and Delle Monache, 1978).

Chalcones **9**–**12**, **16**, and **17** were synthesized according to the procedure described elsewhere (Neves et al., 2012a). The structure elucidation of compounds **3**–**8**, **9**–**12**, **16** and **17** was established on basis of HRMS and NMR techniques. ^{13}C NMR assignments were determined by 2D heteronuclear single quantum correlation (HSQC) and heteronuclear multiple bond correlation (HMBC) experiments. The appearance in the $^{1}HNMR$ spectra of two doublets with a coupling constant ($J_{H\alpha\text{-}H\beta}$) of 15.0–15.6 Hz characteristic of a (*E*)-configuration instead of 12–13 Hz observed for *Z* isomers (Iwata et al., 1997) allowed to confirm that the ethylene moiety in the enone linkage is in the (*E*)-configuration according to previously reported (Balsera et al., 2014; Iwata et al., 1997; Khan et al., 2015; Neves et al., 2012a, 2012b).

3.3. Biological evaluation

3.3.1. Effect in yeast-based screening assay

The best scoring chalcones (docking scores $\leqslant -7$ kcal/mol), which did respect Lipinski rules (AlogP > 5, H-bond donors $\leqslant 5$, H-bond acceptors $\leqslant 10$, and molecular weight < 500), including the newly synthesized chalcones **3**–**6** and those chalcones previously reported by some of us as growth inhibitors of human tumor cell lines (**9**–**12**) (Neves et al., 2012a) were here tested as p53–MDM2 interaction inhibitors. This was carried out using a yeast-based assay previously developed to screen for potential inhibitors of the p53–MDM2 interaction (Leao et al., 2013). In addition, chalcones **7**, **8**, **16**, and **17**, with lower docking scores were also tested in yeast, in order to understand the relationship between docking scores, docking poses, and% of growth inhibition (Table 2). The effectiveness of this yeast assay was recently demonstrated by the discovery of a new inhibitor of the p53–MDM2 interaction with a xanthone (Leao et al., 2013) and an oxazoloisoindolinone (Soares et al., 2015) scaffold. In this yeast assay, the expression of human wt p53 induces yeast growth inhibition, which is abolished by co-expression with human MDM2 (Leao et al., 2013). Inhibitors of the p53–MDM2 interaction, such as nutlin-3A (positive control), reduce the impact of MDM2 on p53 activity, thus restoring the p53-induced yeast growth inhibition. Notably, these small molecules do not interfere with the activity of p53 when expressed alone (Leao et al., 2013). Using this approach, the effect of 1–50 μM of compounds (Table 2) was evaluated using as endpoint the MDM2-dependent reduction of p53-induced yeast growth inhibition. From the concentration–response curves obtained for the tested compounds, 10 μM was selected as the lowest concentration at which a higher reduction of the MDM2 effect was obtained without interfering with the growth of control yeast (empty vectors). Among the tested compounds, only chalcones **3**–**6** and **9**–**12** caused a significant reversion of the inhibitory effect of MDM2 on p53-induced yeast growth inhibition, exhibiting a similar (compounds **5** and **6**) or higher (compounds **3**, **4**, **9**–**12**) effect when compared to nutlin-3A (Table 2). Compounds **3**–**6** and **9**–**12** therefore behaved as potential inhibitors of the p53–MDM2 interaction. On the other hand, compounds **7**, **8**, **16** and **17** were inactive in the yeast assay. It must be noted, that compounds **3**–**6** and **9**–**12** did not interfere with the activity of p53 or MDM2 when expressed alone, nor with the growth of control yeast (vector) (data not shown).

Table 2 Effect of compounds on the inhibitory activity of MDM2 on the p53-induced yeast growth inhibition.

Compounds	Growth Inhibition (% of p53 effect)
DMSO	0.2 ± 4.2
Nutlin-3A	67.8 ± 3.3
3	79.4 ± 4.8
4	97.2 ± 6.3
5	63.7 ± 3.1
6	68.8 ± 2.2
7	19.4 ± 3.4
8	17.4 ± 1.9
9	77.9 ± 7.5
10	95.2 ± 6.8
11	78.3 ± 5.4
12	97.0 ± 4.7
16	0.2 ± 3.2
17	0.1 ± 2.9

Yeast cells expressing p53 and MDM2 were incubated in selective medium in the presence of 10 μM compound or DMSO only, for 42 h. Nutlin-3A was used as positive control. The growth inhibition obtained with yeast cells expressing only p53 treated with dimethyl sulfoxide (DMSO) was considered 100%. Data are mean ± S.E.M. of five independent experiments.

From the 11 compounds predicted by docking studies to be potential p53–MDM2 inhibitors, eight proved to be effective as p53–MDM2 interaction inhibitors in this yeast assay (compounds **3**–**6** and **9**–**12**, 73% success). As expected, chalcones **7**, **8**, **16**, and **17** which presented the lowest docking scores (docking scores > −7 kcal/mol) were found to be inactive or presented low/residual activity in the yeast assay (Table 2).

3.3.2. Effect on human tumor cell lines

3.3.2.1. In vitro cell growth inhibitory activity. In a previous study, two of the most effective p53–MDM2 inhibitors (**10** and **12**) were already shown to have *in vitro* cell growth inhibitory activity in wt p53 human tumor cell lines (Neves et al., 2012a). In this study, compound **10** presented a concentration required to reduce growth rates to 50% of the maximum rate (GI_{50}) lower than 9 μM and compound **12** presented GI_{50} concentrations lower than 47 μM. In the present study, the cell growth inhibitory activities of two of the newly synthesized and most effective p53–MDM2 inhibitors (chalcones **3** and **4**) were analyzed in a panel of human tumor cell lines which included: breast adenocarcinoma MCF-7, non-small cell lung cancer NCI-H460 and gastric adenocarcinoma AGS (all hav-

Table 3 GI_{50} values determined for chalcones **3** and **4** following 48 h of treatment.

	GI_{50} (μM)				
	MCF-7	NCI-H460	AGS	HCT116$^{+/+}$	HCT116$^{-/-}$
Nutlin-3A	–	–	–	3.2 ± 0.1	24.0 ± 0.7
3	2.3 ± 0.1	2.1 ± 0.1	3.2 ± 0.3	2.6 ± 0.2	3.4 ± 0.1
4	3.6 ± 0.3	3.3 ± 0.2	4.5 ± 0.4	5.9 ± 0.4	7.2 ± 1.1

Values, obtained with the Sulforhodamine B assay, refer to the mean ± SEM of at least three independent experiments. The maximum DMSO concentration (0.25%) did not interfere with cell growth (data not shown). Doxorubicin was used as a positive control (GI_{50}: 34.8 ± 7.4 nM in MCF-7, 44.8 ± 13.2 nM in NCI-H460, 59.6 ± 5.1 nM in AGS, 105.5 ± 10.1 nM in HCT-116$^{+/+}$ and >150 nM in HCT-116$^{-/-}$ cells). Values were not determined (–).

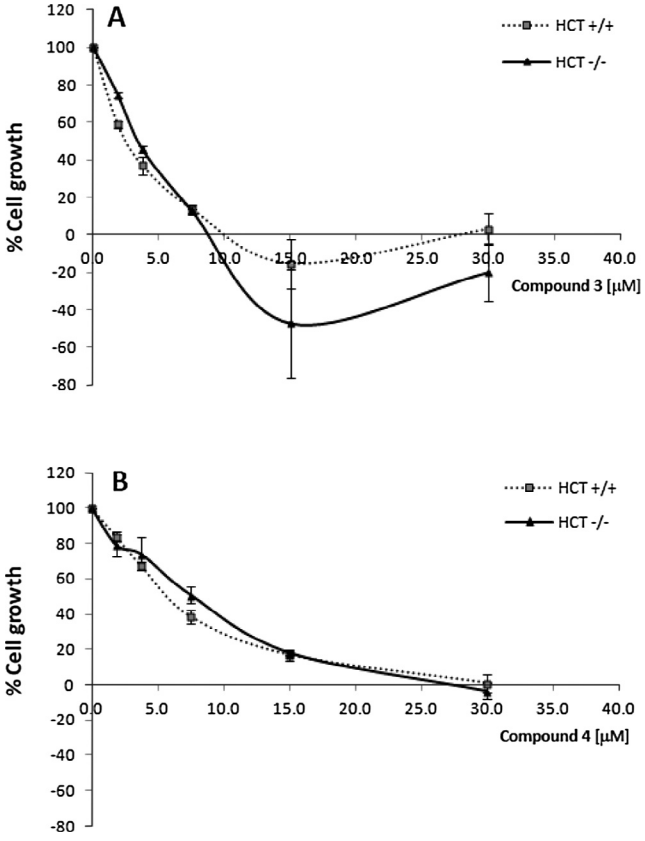

Figure 1 Dose–response curves for compounds **3** (A) and **4** (B), analyzed with SRB assay. HCT116$^{+/+}$ (dashed line) and HCT116$^{-/-}$ (full line) were treated for 48 h with the compounds. Results are the mean ± SEM of, at least, 3 independent experiments.

ing wt p53) (Table 3) and two human colon cancer isogenic HCT116 cell lines, p53$^{+/+}$ and p53$^{-/-}$ (Table 3; Fig. 1).

Results showed that the investigated chalcones inhibited the growth of all the tested cell lines, even of the cell line without p53 (HCT116$^{-/-}$). In fact, contrary to Nutlin-3A, no differences were observed between the GI_{50} concentrations of chalcones **3** and **4** in p53$^{+/+}$ and p53$^{-/-}$ HCT116 cell lines (Table 3), Therefore, in addition to the potential p53–MDM2 inhibitory effect of these compounds, other mechanisms of action may be involved in the growth inhibitory activity observed in human tumor cell lines. In order to

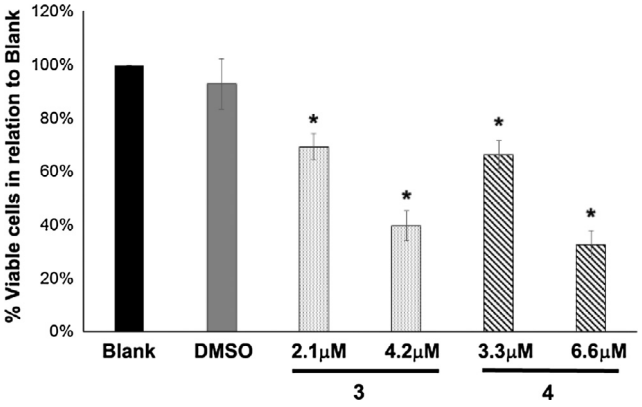

Figure 2 Effect of chalcones **3** and **4** on NCI-H460 viable cell number, analyzed with the trypan blue exclusion assay. Cells were treated for 48 h with the GI_{50} and 2 × GI_{50} concentrations of chalcone **3** (2.1 and 4.2 μM, respectively) and **4** (3.3 and 6.6 μM, respectively) for 48 h. Results are presented as % of viable cells in relation to blank (medium only) and are the mean ± SEM of 4 independent experiments. * $P \leqslant 0.01$ treatment *vs.* Blank.

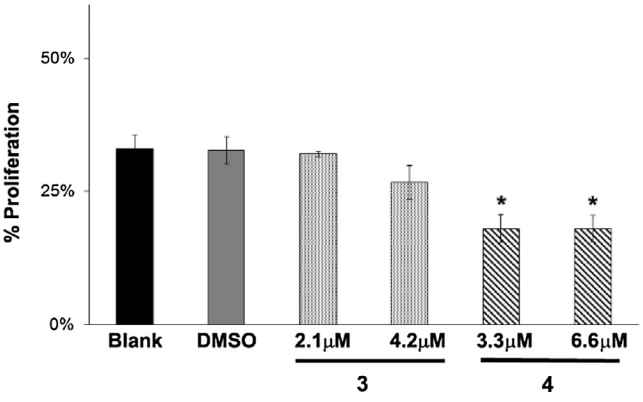

Figure 3 Effect of chalcones **3** and **4** in NCI-H460 cells proliferation. Cells were treated for 48 h with: medium only (Blank), the GI_{50} and 2 × GI_{50} concentrations of chalcone **3** (2.1 and 4.2 μM, respectively) and **4** (3.3 and 6.6 μM, respectively) or with the highest DMSO concentration. Results are the mean ± SEM of the percentage of BrdU-incorporating cells, from at least 3 independent experiments. * $P \leqslant 0.05$ treatment *vs.* Blank.

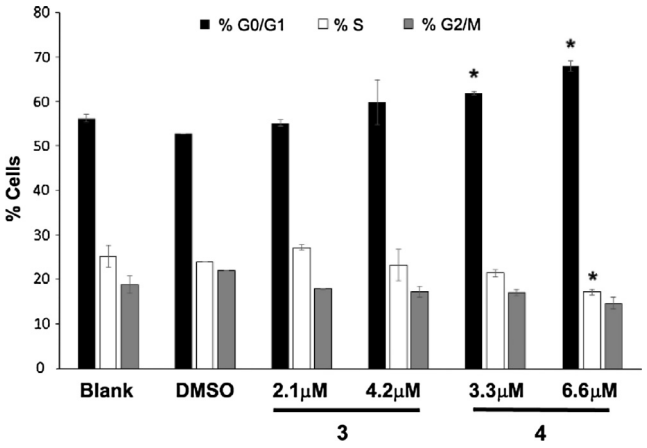

Figure 4 Effect of chalcones **3** and **4** in NCI-H460 cell cycle profile. Cells were treated for 48 h with: medium only (Blank), the GI_{50} and 2 × GI_{50} concentrations of chalcone **3** (2.1 and 4.2 μM, respectively) and **4** (3.3 and 6.6 μM, respectively) or with the highest DMSO concentration. Results are the mean ± SEM of 3 independent experiments. * $P \leqslant 0.01$ treatment *vs.* Blank.

Table 4 Percentage of apoptosis in NCI-H460 cells following treatment with chalcones **3** and **4**.

		% Apoptosis
Blank		9.8 ± 1.1
DMSO		10.0 ± 0.4
3	2.1 μM	9.5 ± 0.9
	4.2 μM	10.1 ± 1.1
4	3.3 μM	15.2 ± 2.5
	6.6 μM	24.3 ± 3.8[a]

Values refer to mean ± SEM of at least 4 independent experiments.
[a] $P \leqslant 0.05$ between treatment *vs.* Blank.

confirm that the growth inhibition induced by chalcones **3** and **4** could occur through p53-dependent pathway activation, their effect was then further investigated in the NCI-H460 cells.

3.3.2.2. Effect on NCI-H460 viable cell number. As expected, treatment with chalcones **3** and **4** significantly decreased NCI-H460 viable cell number, in a dose-dependent manner (Fig. 2). This was observed by counting the number of viable cells with trypan blue exclusion assay 48 h following treatment with the GI_{50} and 2 × GI_{50} concentrations of chalcone **3** (2.1 and 4.2 μM, respectively) and **4** (3.3 and 6.6 μM, respectively). Treatment with DMSO had no effect on cellular viability at the highest concentration tested.

3.3.2.3. Effect on NCI-H460 cellular proliferation and cycle profile. The BrdU incorporation assay was carried out to assess the effect of both chalcones in cellular proliferation. A clear and statistically significant reduction in the levels of proliferation was observed on NCI-H460 cells treated with chalcone **4** (Fig. 3). This was detected by a reduction in the percentage of BrdU-incorporating cells from 33.0% (Blank) to 18.0%

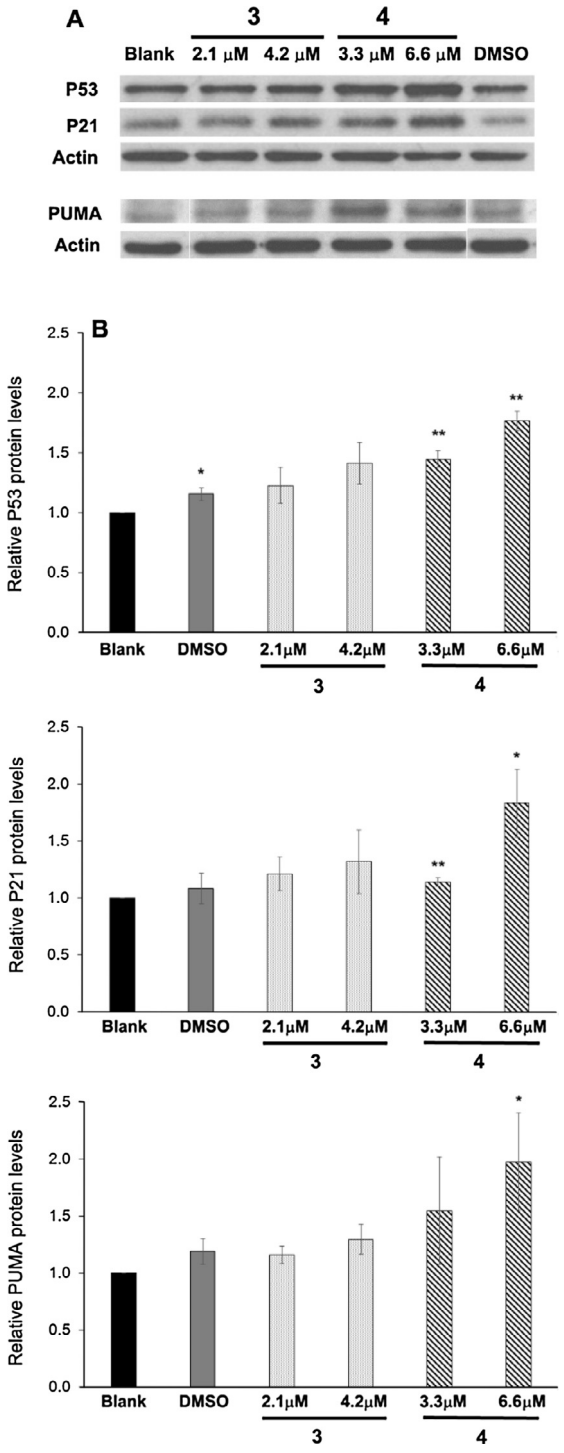

Figure 5 Effects of chalcones **3** and **4** on the levels of p53, p21, and PUMA in NCI-H460 cells. Cells were treated for 48 h with: medium only (Blank), the GI_{50} and 2 × GI_{50} concentrations of chalcone **3** (2.1 and 4.2 μM, respectively) and **4** (3.3 and 6.6 μM, respectively) or with the highest DMSO concentration. Actin was used as loading control. **(A)** Images are representative of at least 3 independent experiments. **(B)** Densitometry analysis of the Western blots. Results are expressed after normalization of the values obtained for each protein with the values obtained for Actin (in relation to Blank cells). Each bar represents the mean ± SEM from, at least, 3 independent experiments. * $P \leqslant 0.05$ and ** $P \leqslant 0.01$ treatment *vs.* Blank.

following treatment with chalcone **4** (at both concentrations analyzed). Regarding chalcone **3**, a small decrease in proliferation (to 25.4%) was noticed with the highest concentration tested (4.2 μM) but was not considered statistically significant.

Furthermore, in order to estimate the percentage of cells in the different phases of the cell cycle, NCI-H460 cells treated with both chalcones were analyzed by flow cytometry after propidium iodide staining. As previously observed for the BrdU incorporation assay, while no alterations were observed in the cell cycle profile of NCI-H460 cells following treatment with chalcone **3**, treatment with chalcone **4** resulted in statistically significant alterations of the NCI-H460 cell cycle profile (Fig. 4). A statistically significant increase in the percentage of cells at the G0/G1 phase, from 56.3% (Blank) to 61.9% and 68.0%, was observed after treatment with chalcone **4** at 3.3 μM and 6.6 μM, respectively. This was accompanied by a decrease in the percentage of cells in the S phase, from 25.2% (Blank) to 17.2% after treatment with 6.6 μM chalcone **4**.

3.3.2.4. Effect on NCI-H460 cellular apoptosis. To evaluate if induction of apoptosis was also involved in the decreased cellular viability observed after treatment with both chalcones, flow cytometric analysis was carried out after labeling cells with Annexin V-FITC/PI. Results showed that chalcone **4** induced apoptosis. This was observed by a dose-dependent increase in the levels of apoptosis to 15.2% and to 24.3%, after treatment with 3.3 μM and 6.6 μM of chalcone **4**, respectively (Table 4).

3.3.2.5. Effect on the levels of p53, p21, and PUMA. Since the previous results showed that chalcone **4** caused cell cycle arrest (mainly at the G0/G1 phase) and induced apoptosis in NCI-H460 cells, which was in agreement with the fact that these compounds were potential inhibitors of p53–MDM2 interaction in the yeast cell model, the expression levels of p53 protein and of some of its downstream targets, p21 and PUMA, were analyzed (Fig. 5).

Results showed an increase in the levels of p53, mainly after treatment with chalcone **4** (Fig. 5). Importantly, the levels of p21 and PUMA were also increased in cells treated with chalcone **4**, further supporting the hypothesis of p53 activation following treatment with chalcone **4.**

3.4. Docking studies

Chalcones **3** and **4** were further analyzed in terms of docking poses and residues involved in the p53–MDM2 potential interaction (Fig. 6).

AutoDock Vina was the software chosen to predict docking conformations and scores, as it has been described as being the best software in predicting crystallographic p53–MDM2 inhibitor poses (RMSD < 1.0 Å) by redocking tests (Bharatham et al., 2014). This was further confirmed by the RMSD comparison between crystallographic and docked nutlin-3A (supplementary data Fig. 1A) and by the establishment of a linear relation between docking scores and% growth inhibition (supplementary data Fig. 1B).

The alpha-helical p53 peptide (residues 18–26) binds to a deep hydrophobic cleft within the amino-terminal domain of MDM2 (Chen et al., 2005). The binding site consists of a larger pocket for Phe-19 and Trp-23 of p53 and a smaller pocket for Leu-26 of p53 (Kalid and Ben-Tal, 2009) (Fig. 6A). Both pockets are mainly hydrophobic. While searching for a chemical moiety that could mimic the interaction between those p53 residues and MDM2, the methoxy-benzene rings of chalcones were found to perfectly mimic the hydrophobic and hydrogen-bonding interactions.

Fig. 6B shows the most stable binding poses of compounds **3** and **4** as suggested by the docking protocol. Compound **4** (Fig. 6**C**), the most active chalcone in the yeast assay and also the one that was predicted to bind more stably *in silico* to MDM2 binding pocket, establishes two hydrogen bond interactions, parallel displaced stacking interactions, dipole–induced dipole and van der Waals interactions, and mimics the key hydrophobic residues of p53 when bound to MDM2. One of the rings of the chalcone moiety of **4** occupies the Leu-26 subpocket and forms two hydrogen bond interactions with the protein. The other ring occupies the subpockets Phe-19/Trp-23. This expanded conformation and scaffold orientation in the cleft where p53 is supposed to bind, allows

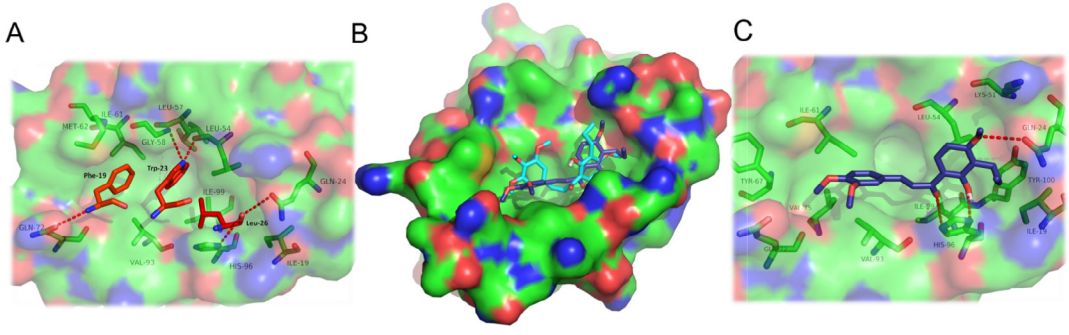

Figure 6 (A**)** Binding mode of crystallographic p53 (for simplification, only residues Phe-19, Trp-23, and Leu-26, are represented as red sticks). (B**)** MDM2 (solid surface) interacting with p53 (transparent surface) via Phe-19, Trp-23, and Leu-26 (red sticks) side chains that fit into three corresponding pockets on the protein. (A) The most potent chalcones tested as p53–MDM2 interaction inhibitors (3, 4; represented in blue sticks) docked into MDM2 structure, as predicted by the docking studies. (C**)** Predicted binding poses of compound 4 (blue sticks) in the binding site of MDM2. Structural data were obtained from PDB structures 4HG7 and 1YCR. MDM2 is represented as surface, where carbon, oxygen, nitrogen, and sulfur are represented in green, red, blue, and yellow, respectively. Hydrogen interactions are depicted with a dashed red line. Residues involved in other interactions are represented as green sticks.

additional interactions to be formed, strengthening the bonding. Although no hydrogen interactions are predicted to be established between **4** and subpockets Phe-19 and Trp-23 (Fig. 6C), induced dipole–permanent dipole, hydrophobic, and van der Waals interactions occur between the substituted chalcone rings and those subpockets. These types of interactions are also described as being important for MDM2:p53 complexation (Zhao et al., 2015). However, Trp-23 is only partially occupied by **4** (only Leu-54 establishes interaction with the small molecule), leaving most of the pocket empty (Fig. 6C). The inactive derivatives (**7** and **8**) and the derivatives with low activity in the yeast assay are predicted to bind to MDM2 in a different location and conformation (not shown). From the docking results, it should be highlighted that more hindered rings, with methoxyl and propyl substituents are predicted to orient the molecule in the binding site in a more expanded conformation, occupying a larger volume of the binding pocket and establishing more hydrogen and van der Waals interactions. This information could lead to a new family of chalcones, which may bind with more affinity to the Mdm2 protein; from the docking results it is induced that more hindered A rings, with additional polar groups at positions 5 and 6, would allow the establishment of the lacking hydrogen interactions with Trp-23 subpocket.

4. Conclusion

In this work, using virtual screening followed by analysis of the biological activity of the selected compounds in a yeast-based screening assay, eight chalcones (**3**–**6** and **9**–**12**) were identified for the first time as p53–MDM2 interaction inhibitors. The *in vitro* antitumor activity of two of the most effective compounds (**3** and **4**) was further confirmed in human tumor cell lines, in which chalcone **4** growth inhibitory effect was clearly associated to an activation of the p53 pathway. Nevertheless, these compounds might have other mechanisms of action which are independent from p53, which would explain the similar GI_{50} concentrations obtained in the HCT116 $p53^{+/+}$ and $p53^{-/-}$ isogenic cells. The p53-independent mechanisms that may also be implicated in their mechanism of action need further confirmation. In the future, other chalcone derivatives with *n*-propyl groups at ring A, and with additional rings linked to ring B will be synthetized and tested. The results obtained from this study will be valuable for the rational design of novel and potent p53–MDM2 inhibitors.

Acknowledgments

This research was partially supported by the Strategic Funding UID/Multi/04423/2013, ERDF, COMPETE, and FCT under the projects PTDC/MAR-BIO/4694/2014, and INNOVMAR – Innovation and Sustainability in the Management and Exploitation of Marine Resources, reference NORTE-01-0145-FEDER-000035, Research Line NOVELMAR. This work also received financial support from the European Union (FEDER funds POCI/01/0145/FEDER/007265) and National Funds (FCT/MEC, Fundação para a Ciência e Tecnologia and Ministério da Educação e Ciência) under the Partnership Agreement PT2020 UID/QUI/50006/2013 and the FCT project PTDC/DTP-FTO/1981/2014, "PEst-C/SAU/LA0003/2013", "NORTE-07-0162-FEDER-00018 – Contributos para o reforço da capacidade do IPATIMUP enquanto actor do sistema regional de inovação" and NORTE-07-0162-FEDER-000067 – Reforço e consolidação da capacidade infraestrutural do IPATIMUP para o sistema regional de inovação", both supported by ON.2 – O Novo Norte, through FEDER funds under the QREN. IPATIMUP integrates the i3S Research Unit, which is partially supported by FCT. The authors also thank FCT for the grants of R.T. Lima (SFRH/BPD/68787/2010), J. Soares (SFRH/BD/78971/2011), and S. Gomes (SFRH/BD/96189/2013; Doctoral Programme BiotechHealth), L. Raimundo (PD/BI/113926/2015, Doctoral Programme BiotechHealth).

Appendix A. Supplementary data

Supplementary data associated with this article can be found, in the online version, at http://dx.doi.org/10.1016/j.arabjc.2016.04.015.

References

Alves de Lima, R., Delle Monache, G., Botta, B., 1982. Pyridine-d5 induced shift in PMR spectra as a base for structural elucidation of natural polyphenols. Rev. Latinoam. Quim. 13 (2), 61–64.

Alves de Lima, R., Delle Monache, G., 1978. Studies on flavones Acetophenones as model compounds for analyzing flavonoids using UV and NMR spectroscopy. Rendiconti – Accademia Nazionale dei 40 (Quaranta 3), 181–191.

Anil, B., Riedinger, C., Endicott, J.A., Noble, M.E., 2013. The structure of an MDM2-Nutlin-3a complex solved by the use of a validated MDM2 surface-entropy reduction mutant. Acta Crystallogr. D Biol. Crystallogr. 69 (Pt 8), 1358–1366.

Balsera, B., Mulet, J., Fernandez-Carvajal, A., de la Torre-Martinez, R., Ferrer-Montiel, A., Hernandez-Jimenez, J.G., Estevez-Herrera, J., Borges, R., Freitas, A.E., Lopez, M.G., Garcia-Lopez, M.T., Gonzalez-Muniz, R., Perez de Vega, M.J., Valor, L.M., Svobodova, L., Sala, S., Sala, F., Criado, M., 2014. Chalcones as positive allosteric modulators of alpha7 nicotinic acetylcholine receptors: a new target for a privileged structure. Eur. J. Med. Chem. 86, 724–739.

Bharatham, N., Bharatham, K., Shelat, A.A., Bashford, D., 2014. Ligand binding mode prediction by docking: MDM2/MDMx inhibitors as a case study. J. Chem. Inf. Model. 54 (2), 648–659.

Cazal, C.M., Choosang, K., Severino, V.G., Fernandes, J.B., Silva, A. M., Vieira, P.C., Nascimento, M.S., Almeida, G.M., Vasconcelos, M.H., Pakkong, P., Pinto, M., 2013. Natural compounds with cell growth inhibitory activity in human tumor cell lines. Antican. Agents Med. Chem. 13 (10), 1582–1589.

Chen, L., Yin, H., Farooqi, B., Sebti, S., Hamilton, A.D., Chen, J., 2005. P53 alpha-Helix mimetics antagonize p53/MDM2 interaction and activate p53. Mol. Can. Ther. 4 (6), 1019–1025.

Erlund, I., 2004. Review of the flavonoids quercetin, hesperetin, and naringenin. Dietary sources, bioactivities, bioavailability, and epidemiology. Nut. Res. 24 (10), 851–874.

Ferreira, A., Pousinho, S., Fortuna, A., Falcão, A., Alves, G., 2014. Flavonoid compounds as reversal agents of the P-glycoprotein-mediated multidrug resistance: biology, chemistry and pharmacology. Phytochem. Rev.

Fotouhi, N., Graves, B., 2005. Small molecule inhibitors of p53/MDM2 interaction. Curr. Top. Med. Chem. 5 (2), 159–165.

Froimowitz, M., 1993. HyperChem: a software package for computational chemistry and molecular modeling. Biotechniques 14 (6), 1010–1013.

Ghose, A.K., Crippen, G.M., 1987. Atomic physicochemical parameters for three-dimensional structure-directed quantitative structure-activity relationships I. Partition coefficients as a measure of hydrophobicity. J. Chem. Inf. Comput. Sci. 27 (1), 21–35.

Iwata, S., Nishino, T., Inoue, H., Nagata, N., Satomi, Y., Nishino, H., Shibata, S., 1997. Antitumorigenic activities of chalcone (II).

Photo-isomerization of chalcones and the correlation with their biological activities. Biol. Pharm. Bull. 20, 1266–1270.
Kalid, O., Ben-Tal, N., 2009. Study of MDM2 binding to p53-analogues: affinity, helicity, and applicability to drug design. J. Chem. Inf. Model. 49 (4), 865–876.
Kamal, A., Mohammed, A.A., Shaik, T.B., 2012. P53–MDM2 inhibitors: patent review (2009–2010). Expert Opin. Ther. Pat. 22 (2), 95–105.
Khan, S.A., Asiri, A.M., Basisi, H.M., 2015. Synthesis, single X-ray crystal, spectroscopic and photophysical studies of novel heterocyclic chalcones with their biological application. J. Fluoresc. 25 (4), 825–834.
Kussie, P.H., Gorina, S., Marechal, V., Elenbaas, B., Moreau, J., Levine, A.J., Pavletich, N.P., 1996. Structure of the MDM2 oncoprotein bound to the p53 tumor suppressor transactivation domain. Science 274 (5289), 948–953.
Lai, C.K., Rao, Y.K., Chang, K.R., Lin, C.W., Su, H.L., Chang, C.S., Lai, C.H., Tzeng, Y.M., 2014. 3,3′,4′, 5′-Tetramethoxychalcone inhibits human oral cancer cell proliferation and migration via p53-mediated mitochondrial-dependent apoptosis. Antican. Res. 34 (4), 1811–1819.
Leao, M., Pereira, C., Bisio, A., Ciribilli, Y., Paiva, A.M., Machado, N., Palmeira, A., Fernandes, M.X., Sousa, E., Pinto, M., Inga, A., Saraiva, L., 2013. Discovery of a new small-molecule inhibitor of p53–MDM2 interaction using a yeast-based approach. Biochem. Pharmacol. 85 (9), 1234–1245.
Lill, M.A., Danielson, M.L., 2010. Computer-aided drug design platform using PyMOL. J. Comput. Aided Mol. Des. 25 (1), 13–19.
Lima, R.T., Martins, L.M., Guimaraes, J.E., Sambade, C., Vasconcelos, M.H., 2006. Chemosensitization effects of XIAP downregulation in K562 leukemia cells. J. Chemother. 18 (1), 98–102.
Ma, B., Pan, Y., Gunasekaran, K., Keskin, O., Venkataraghavan, R. B., Levine, A.J., Nussinov, R., 2005. The contribution of the Trp/Met/Phe residues to physical interactions of p53 with cellular proteins. Phys. Biol. 2 (2), S56–S66.
Mahapatra, D.K., Bharti, S.K., Asati, V., 2015. Anti-cancer chalcones: structural and molecular target perspectives. Eur. J. Med. Chem. 98, 69–114.
Neves, M.P., Cidade, H., Pinto, M., Silva, A.M., Gales, L., Damas, A. M., Lima, R.T., Vasconcelos, M.H., de Sao Jose Nascimento, M., 2011. Prenylated derivatives of baicalein and 3,7-dihydroxyflavone: synthesis and study of their effects on tumor cell lines growth, cell cycle and apoptosis. Eur. J. Med. Chem. 46 (6), 2562–2574.
Neves, M.P., Cravo, S., Lima, R.T., Vasconcelos, M.H., Nascimento, M.S., Silva, A.M., Pinto, M., Cidade, H., Correa, A.G., 2012a. Solid-phase synthesis of 2′-hydroxychalcones. Effects on cell growth inhibition, cell cycle and apoptosis of human tumor cell lines. Bioorg. Med. Chem. 20 (1), 25–33.
Neves, M.P., Lima, R.T., Choosang, K., Pakkong, P., de Sao Jose Nascimento, M., Vasconcelos, M.H., Pinto, M., Silva, A.M., Cidade, H., 2012b. Synthesis of a natural chalcone and its prenyl analogs–evaluation of tumor cell growth-inhibitory activities, and effects on cell cycle and apoptosis. Chem. Biodiv. 9 (6), 1133–1143.
Paiva, A.M., Pinto, R.A., Teixeira, M., Barbosa, C.M., Lima, R.T., Vasconcelos, M.H., Sousa, E., Pinto, M., 2013. Development of noncytotoxic PLGA nanoparticles to improve the effect of a new inhibitor of p53–MDM2 interaction. Int. J. Pharm. 454 (1), 394–402.
Preto, A., Goncalves, J., Rebocho, A.P., Figueiredo, J., Meireles, A. M., Rocha, A.S., Vasconcelos, H.M., Seca, H., Seruca, R., Soares, P., Sobrinho-Simoes, M., 2009. Proliferation and survival molecules implicated in the inhibition of BRAF pathway in thyroid cancer cells harbouring different genetic mutations. BMC Can. 9, 387.
Rao, Y.K., Kao, T.-Y., Ko, J.-L., Tzeng, Y.-M., 2010. Chalcone HTMC causes in vitro selective cytotoxicity, cell-cycle G1 phase arrest through p53-dependent pathway in human lung adenocarcinoma A549 cells, and in vivo tumor growth suppression. Bioorg. Med. Chem. Lett. 20 (22), 6508–6512.
Sahu, N.K., Balbhadra, S.S., Choudhary, J., Kohli, D.V., 2012. Exploring pharmacological significance of chalcone scaffold: a review. Curr. Med. Chem. 19 (2), 209–225.
Secchiero, P., Bosco, R., Celeghini, C., Zauli, G., 2011. Recent advances in the therapeutic perspectives of Nutlin-3. Curr. Pharm. Des. 17 (6), 569–577.
Seeliger, D., de Groot, B.L., 2010. Ligand docking and binding site analysis with PyMOL and Autodock/Vina. J. Comput. Aided Mol. Des. 24 (5), 417–422.
Selivanova, G., 2014. Wild type p53 reactivation: from lab bench to clinic. FEBS Lett. 588 (16), 2628–2638.
Singh, P., Anand, A., Kumar, V., 2014. Recent developments in biological activities of chalcones: a mini review. Eur. J. Med. Chem. 85, 758–777.
Smejkal, K., 2014. Cytotoxic potential of C-prenylated flavonoids. Phytochem. Rev. 13, 245–275.
Soares, J., Pereira, N.A.L., Monteiro, Â., Leão, M., Bessa, C., dos Santos, D.J.V.A., Raimundo, L., Queiroz, G., Bisio, A., Inga, A., Pereira, C., Santos, M.M.M., Saraiva, L., 2015. Oxazoloisoindolinones with in vitro antitumor activity selectively activate a p53-pathway through potential inhibition of the p53–MDM2 interaction. Eur. J. Pharm. Sci. 66, 138–147.
Stoll, R., Renner, C., Hansen, S., Palme, S., Klein, C., Belling, A., Zeslawski, W., Kamionka, M., Rehm, T., Muhlhahn, P., Schumacher, R., Hesse, F., Kaluza, B., Voelter, W., Engh, R.A., Holak, T.A., 2001. Chalcone derivatives antagonize interactions between the human oncoprotein MDM2 and p53. Biochemistry 40 (2), 336–344.
Trott, O., Olson, A.J., 2009. AutoDock Vina: improving the speed and accuracy of docking with a new scoring function, efficient optimization, and multithreading. J. Comput. Chem. 31 (2), 455–461.
Vousden, K.H., Prives, C., 2009. Blinded by the light: the growing complexity of p53. Cell 137 (3), 413–431.
Wang, S., Zhao, Y., Bernard, D., Aguilar, A., Kumar, S., 2012. Targeting the MDM2–p53 protein–protein interaction for new cancer therapeutics. Top. Med. Chem. 8, 57–80.
Wang, Y., Xiao, J., Suzek, T.O., Zhang, J., Wang, J., Bryant, S.H., 2009. PubChem: a public information system for analyzing bioactivities of small molecules. Nucl. Acids Res. 37 (Web Server issue), 623–633.
Zhao, Y., Aguilar, A., Bernard, D., Wang, S., 2015. Small-molecule inhibitors of the MDM2–p53 protein-protein interaction (MDM2 Inhibitors) in clinical trials for cancer treatment. J. Med. Chem. 58 (3), 1038–1052.
Zhou, Y., Ho, W.S., 2014. Combination of liquiritin, isoliquiritin and isoliquirigenin induce apoptotic cell death through upregulating p53 and p21 in the A549 non-small cell lung. Oncol. Rep. 31 (1), 298–304.